NJC

Magnetic anisotropies and slow magnetic relaxation of three tetrahedral tetrakis(pseudohalido)-cobalt(II) complexes

Journal:	*New Journal of Chemistry*
Manuscript ID	NJ-ART-04-2021-001916.R2
Article Type:	Paper
Date Submitted by the Author:	06-Aug-2021
Complete List of Authors:	Chen, Shuyang; Nanjing University, School of Chemistry and Chemical Engineering, Lv, Wei; Coordination Chemistry Institute, State Key Laboratory of Coordination Chemistry Cui, Hui-Hui; Coordination Chemistry Institute, State Key Laboratory of Coordination Chemistry Chen, Lei; Jiangsu University of Science and Technology, School of Environmental and Chemical Engineering Zhang, Yi-Quan; School of Physical Science and Technology, Physical department Chen, Xue-tai; Coordination Chemistry Institute, State Key Laboratory of Coordination Chemistry; Wang, Zhenxing; Huazhong University of Science and Technology, Wuhan National High Magnetic Field Center; Ouyang, Zhongwen; National High Magnetic Field Center, Huazhong University of Science and Technology, Yan, Hong; Nanjing University, State Key Laboratory of Coordination Chemistry Xue, Zi-Ling; University of Tennessee, Department of Chemistry

ARTICLE

Magnetic anisotropies and slow magnetic relaxation of three tetrahedral tetrakis(pseudohalido)-cobalt(II) complexes

Received 00th January 20 xx,
Accepted 00th January 20 xx

DOI: 10.1039/x0xx00000x

Shu-Yang Chen,[a] Wei Lv,[a] Hui-Hui Cui,[a] Lei Chen,[b] Yi-Quan Zhang,*[c] Xue-Tai Chen,*[a] Zhenxing Wang,*[d], Zhong-Wen Ouyang,[d] Hong Yan*[a] and Zi-Ling Xue[e]

Three mononuclear tetrakis(pseudohalido)-cobalt(II) complexes $(Ph_4P)_2[Co(E)_4]$ (E = N_3^-, **1**; NCO^-, **2**; NCS^-, **3**) have been synthesized and structurally characterized. Each compound contains a distorted tetrahedral Co^{2+} ion coordinated by four pseudohalide ligands. The magnetic properties of **1**-**3** have been studied by direct-current magnetic measurements and high-frequency and -field EPR spectroscopy (HFEPR), suggesting the easy-axis magnetic anisotropy for **1** and **2** and easy-plane anisotropy for **3**. The analyses of HFEPR spectra have yielded *D* values of –5.23 and +3.63 cm^{-1} for **2** and **3**, respectively. The absence of the EPR signal in **1** is consistent with a large, negative value of the zero-field splitting (ZFS) parameter *D* in **1**. The nature of magnetic anisotropies of **1**-**3** have also been confirmed by the *ab initio* calculations. The calculated *D* values are consistent with those determined by magnetometry and HFEPR studies. Alternating-current (ac) magnetic susceptibilities reveal the slow magnetic relaxation under an applied magnetic field, thus indicating that **1**-**3** are field-induced single-ion magnets (SIMs).

Introduction

Single-molecule magnets (SMMs), which display slow magnetic relaxation at low temperatures, have been intensively studied in the last three decades because of their potential applications in quantum computation, high density information storage and molecular spintronics.[1] The initial research effects were focused on SMMs based on polynuclear metal complexes since the discovery of Mn_{12}-acetate as the first SMM.[2] Subsequent studies proved difficult to simultaneously enhance magnetic anisotropies and enlarge spin numbers in the polynuclear complexes, which were responsible for the SMM properties.[3] Recent studies have turned to the SMMs containing a single paramagnetic ion, which are referred to as single-ion magnets (SIMs). Studies of lanthanide-ion SIMs[4] have also led to major recent progresses, as the blocking temperature of $[Cp^{iPr5}]Dy(Cp^*)]^+$, for example, reaches 80 K.[4b] Compared to lanthanide-ion SIMs,[4] the transition metal ion SIMs exhibit lower energy barrier for spin reversal due to their small magnetic anisotropies. However, a transition metal ion SIM generally provides a simpler case to fine-tune magnetic anisotropy through adjusting the donor atom, coordination number and geometry. In transition metal complexes, strong metal-ligand interaction often quenches the first-order orbital contributions to the magnetic moment. As a result, the magnetic anisotropy arises from the second-order spin-orbit coupling (SOC), which can be depicted by the effective spin-Hamiltonian.[5] To date, various transition metal complexes containing 3*d* ions[5-15] have been found to display slow magnetic relaxation, among which Co(II)-based SIMs form the largest family with various configurations and coordination numbers from two to eight.[5-15]

Four-coordinate tetrahedral Co(II)-based SIMs are particularly attractive.[8-11] The tetrahedral geometry splits the *d* orbitals of the Co(II) ion to produce a small energy gap between the ground and excited states, facilitating the SOC and thus promoting magnetic anisotropy.[8-11] The four-coordinate Co(II)-SIMs usually contain a mixed donor set from N, P, As, O, S, Se and/or halides.[8] A smaller number of homoleptic SIMs containing a CoX_4 unit (X = O, S, Se, Te,[9] N,[10] Cl[11]) with four identical donors have been reported, as summarized in Table S1 (ESI†). Since mixed donors could induce additional anisotropy,[8] homoleptic four-coordinate Co(II) complexes could be better candidates to study the correlations between donor atoms and magnetic anisotropy.

[a] State Key Laboratory of Coordination Chemistry, School of Chemistry and Chemical Engineering, Nanjing University, Nanjing 210023, China. E-mail: xtchen@nju.edu.cn; hyan1965@nju.edu.cn
[b] School of Environmental and Chemical Engineering, Jiangsu University of Science and Technology, Zhenjiang 212003, China.
[c] Jiangsu Key Laboratory for NSLSCS, School of Physical Science and Technology, Nanjing Normal University, Nanjing 210023, China. Email: zhangyiquan@njnu.edu.cn
[d] Wuhan National High Magnetic Field Center & School of Physics, Huazhong University of Science and Technology, Wuhan 430074, China. Email: zxwang@hust.edu.cn
[e] Department of Chemistry, University of Tennessee, Knoxville, Tennessee 37996, USA.

Electronic Supplementary Information (ESI) available: XRD patterns, calculation results and magnetic data. See DOI: 10.1039/x0xx00000x

Several studies have been performed on the effect of the donor atoms of the congeners on magnetic anisotropy.[8c-8g,9b] Specifically, the effect of pseudo-halide ligands on magnetic properties of Co(II) complexes has been investigated.[8f,16] Switlicka *et al*. found easy-axis anisotropy for $[Co(bmin)_2(X)_2]$ (bmin = 1-benzyl-2-methylimidazole, X = NCS^-) and easy-plane anisotropy for the analogues with X = NCO^-, N_3^- using the magnetometry and theoretical calculations.[8f] Krzystek *et al*. have revealed the sensitivity of the ZFS parameter *D* in the series of complexes $Tp^{R,R'}CoX$ ($Tp^{R,R'}$ = hydrotris(3-R,5-R′-pyrazol-1-yl)borate anion, X = NCS^-, NCO^-, N_3^-) by HFEPR.[16]

A CSD search (Cambridge Structural Database, Version 5.42) revealed 114, 12 and 2 structures for the complexes containing anions $[Co(NCS)_4]^{2-}$,[17] $[Co(NCO)_4]^{2-}$,[18] and $[Co(N_3)_4]^{2-}$,[19] respectively. They are summarized in Tables S2-S4. Only a few complexes, listed in Table 1, have been magnetically studied.[10e-10h] Gao *et al*. reported slow magnetic relaxation in two Co(II)-SIMs containing the $[Co(NCS)_4]^{2-}$ anion, $[K(18C6)]_2[Co(NCS)_4]$ (18C6 = 18-crown-6) and $[Ba(18C6)\cdot 3H_2O][Co(NCS)_4]$, which exhibit weak easy plane anisotropies with *D* values of +2.57 and +5.56 cm^{-1}, respectively, as determined by HFEPR.[10e] Later, slow magnetic relaxation was revealed for the same magnetic anions with square-planar $[Ni(Me_6trans[14]dieneN_4)]^{2+}$ ($Me_6trans[14]dieneN_4$ = 5,7,7,12,14,14-hexamethyl-1,4,8,11-tetraazacyclotetradeca-4,11-diene) cations[10f] and a spin-crossover Co(II) cation $[Co(Brphterpy)_2]^{2+}$ (Brphterpy = 4′-(4′-bromo-biphenyl-4-yl) -[2,2′:6′,2″]terpyridine), whose *D* values were estimated to be positive.[10g] The tetrakis(cyanato)-Co(II) anions $[Co(NCO)_4]^{2-}$ and $[Co(NCS)_4]^{2-}$ containing a spin-crossover cation $[Co(tppz)_2]^{2+}$ (tppz = 2,3,5,6-tetrakis-(2-pyridyl)pyrazine) exhibit weak easy-plane anisotropy.[10h] These reported examples of complexes with the $[Co(NCS)_4]^{2-}$ and $[Co(NCO)_4]^{2-}$ anions are listed in Table 1. Similar to NCS^- and NCO^-, the azido ligand is also an important pseudohalide in magnetic complexes.[12b] However, the magnetic property of the complexes containing the tetrakis(azido)-Co(II) anion has been not studied yet.

Table 1 Summary of the magnetic properties of $[Co(NCX)_4]^{2-}$ complexes with different cations

complex	*D* (cm^{-1})	*E* (cm^{-1})	SIM[d]	Deviation parameters	Ref.
$[K(18C6)]_2[Co(NCS)_4]$	+2.57[a]	0.82[a]	Yes	0.036	10*e*
$[Ba(18C6)\cdot 3H_2O][Co(NCS)_4]$	+5.56[a]	1.05[a]	Yes	0.101	10*e*
$HgCo(NCS)_4$	+5.39[a]	0	Yes	0.503	20
$[Ni(Me_6trans[14]dieneN_4)][Co(NCS)_4]$	+3.74[b]	0.051[b]	No	0.042	10*f*
$[Ni(Me_6trans[14]dieneN_4)]_2[Co(NCS)_4](ClO_4)_2\cdot H_2O$	+11.6[b]	0.023[b]	Yes	1.506	10*f*
$[Ni(Me_6trans[14]dieneN_4)]_2[Co(NCS)_4](PF_6)_2$	+7.29[b]	0.50[b]	Yes	1.343	10*f*
$[Co(tppz)_2][Co(NCS)_4]\cdot MeOH$	+3.8[b]	0[c]	No	0.472	10*h*
$[Co(Brphterpy)_2][Co(NCS)_4]\cdot 2MeCN$	+7.55[b]	0.01[b]	Yes	0.199	10*g*
$(Ph_4P)_2[Co(NCS)_4]$ (**3**)	+3.63[a]	0.49[a]	Yes	0.055	This Work
$[Co(tppz)_2][Co(NCO)_4]\cdot 2H_2O$	+4.3[b]	0[c]	Yes	0.184	10*h*
$(Ph_4P)_2[Co(NCO)_4]$ (**2**)	-5.23[a]	0.056[a]	Yes	0.073	This Work

Note: *a*. *D* and *E* determined by HFEPR spectra; *b*. *D* and *E* values estimated by magnetic data; *c*. The *E* value was assumed to be zero; *d*. "Yes" and "No" mean if the slow magnetic relaxation is observed or not by the conventional SQUID. $Me_6trans[14]dieneN_4$ = 5,7,7,12,14,14-hexamethyl-1,4,8,11-tetraazacyclotetradeca-4,11-diene; tppz = 2,3,5,6-tetrakis-(2-pyridyl)pyrazine; Brphterpy = 4′-(4′-bromo-biphenyl-4-yl)-[2,2′:6′,2″]terpyridine.

Considering that the counter ion has an effect on magnetic properties of SIMs, we have prepared and characterized three four-coordinate Co(II) complexes with the same counter-cation Ph_4P^+, $(Ph_4P)_2[Co(E)_4]$ (E = N_3^-, **1**; NCO^-, **2**; NCS^-, **3**). They have similar tetrahedral geometries with a CoN_4 unit. Detailed dc magnetic measurements and HFEPR spectra have been used to study their magnetic anisotropies. The ac magnetic susceptibility studies show that **1-3** are field-induced SIMs. The results are reported herein.

Experimental Section

General information

Materials and methods

All starting reagents were used as received from commercial sources without further purification. The infrared spectra were measured in the range of 400-4000 cm^{-1} on a Tensor 27 FT-IR spectrometer using KBr pellets. Elemental analyses (C, H, and N) were performed on an Elementar Vario ELIII elemental analyzer. The powder XRD patterns were recorded on a Bruker D8 Advance X-ray powder diffractometer at a voltage of 40 kV and a current of 40 mA in the 2θ range of 5-50° at room temperature (Figs. S1-S3, ESI). HFEPR experiments were performed using a spectrometer constructed at the National High Magnetic Field Laboratory, USA.[21]

Synthesis of complexes 1-3

Caution! Metal azide complexes are potentially explosive and should be handled in small quantities with care.

$[Ph_4P]_2[CoCl_4]$. This compound was synthesized according to the published procedure.[22] A solution of Ph_4PCl (0.75 g, 2.0 mmol) in ethanol (3 mL) was added under stirring to a solution of $CoCl_2\cdot 6H_2O$ (0.24 g, 1.0 mmol) in hot ethanol (3 mL). Blue powder precipitated immediately. The resulting

solid (0.79 g, 90% yield) was filtered off, dried under reduced pressure, and used for the further reactions.

$[Ph_4P]_2[Co(N_3)_4]$ (1). An excess of NaN_3 (0.50 g, 7.7 mmol) was slowly added to a solution of $[Ph_4P]_2[CoCl_4]$ (0.25 g, 0.28 mmol) in acetone (10 mL). The mixture was allowed to stir overnight at room temperature. Then it was filtered and concentrated to 5 mL. The vapour of absolute ether was diffused into the concentrated filtrate to give diffraction-quality blue crystals of **1** in 78% yield. Anal. Calc. (%) for $C_{48}H_{40}CoN_{12}P_2$: C, 63.65; H, 4.45; N, 18.56. Found: C, 63.86; H, 4.78; N, 18.20%. IR (cm^{-1}): 3347 (w), 3080 (w), 2048 (s), 1721 (w), 1655 (w), 1585 (w), 1483 (w), 1435 (m), 1345 (w), 1108 (s), 995 (w), 758 (w), 723 (s), 691 (m), 527 (s).

$[Ph_4P]_2[Co(NCO)_4]$ (2). Blue crystals of **2** were prepared by a procedure similar to that used to make **1**, except the same equivalent KNCO used instead of NaN_3. Yield 74%. Anal. Calc. (%) for $C_{52}H_{40}CoN_4P_2O_4$: C, 68.95; H, 4.45; N, 6.19. Found: C, 69.00; H, 4.50; N, 6.19%. IR (cm^{-1}): 3130 (m), 2207 (s), 1680 (w), 1584 (w), 1482 (m), 1438 (s), 1401 (s), 1320 (m), 1186(w), 1107 (s), 996 (w), 758 (w), 723 (s), 690 (m), 613 (m), 526 (s).

$[Ph_4P]_2[Co(NCS)_4]$ (3). Blue crystals of **3** were prepared by a procedure similar to that used to make **1**, except the same equivalent KNCS used instead of NaN_3. Yield 77%. Anal. Calc. (%) for$C_{52}H_{40}CoN_4P_2S_4$: C, 64.38; H, 4.16; N, 5.78. Found: C, 64.38; H, 4.15; N, 5.74%. IR (cm^{-1}): 3131 (m), 2079 (s), 1678 (w), 1582 (w), 1480 (w), 1436 (m), 1400 (s), 1316 (w), 1186(w), 1105 (s), 995 (w), 753 (w), 722 (s), 688 (m), 527 (s), 474 (w).

X-ray single-crystal structure determinations

Single crystal X-ray diffraction data were collected on a Bruker SMART APEX II diffractometer with a CCD area detector (Mo-K_α radiation, λ = 0.71073 Å) at 296 K. The APEX II program was used to determine the lattice parameters and for data collection. The data were integrated and corrected using SAINT.[23] The absorption corrections were applied using the 'multi-scan' method with SADABS.[24] The structures were solved by the direct methods and refined on F^2 by full-matrix least squares using SHELXL (version 2018/3).[25] All non-hydrogen atoms were refined with anisotropic thermal parameters, and all hydrogen atoms were located at calculated positions and generated by the riding model.

Magnetic measurements

Magnetic measurements were performed on polycrystalline samples restrained in a frozen eicosane matrix using a Quantum Design SQUID VSM magnetometer. Dc magnetic data were recorded at fields up to 7 T in the range of 1.8-300 K under an applied dc field of 0.1 T. Ac susceptibility measurements were carried out under an oscillating ac field of 0.2 mT and ac frequencies ranging from 1 to 1000 Hz. Dc magnetic susceptibilities were corrected for diamagnetism using Pascal constants[26] and a sample holder correction.

Results and discussion

Structural features

Single-crystal X-ray diffraction analyses show that **1-3** crystallize in the monoclinic $P2_1/n$ or $C2/c$ space group (Table S5). The structures of the anions are depicted in Fig. 1. Selected bond lengths and bond angles are given in Table 2. It is noted that the crystal structure of a polymorphic form of **1** has been reported.[19a]

As shown in Fig. 1, the Co(II) ion is coordinated by four nitrogen atoms from pseudohalido ligands to form a distorted tetrahedral geometry.

In **1**, one of the four azido ligands is disordered and can be located in two positions. The Co-N bond lengths fall in the range 1.947(15)-1.995(4) Å, which are longer than those in **2** (1.956(2)-1.976(3) Å) and **3** (1.943(2)-1.949(3) Å). These Co-N bond length differences among **1-3** could be due to the coordination abilities of these three pseudohalides.

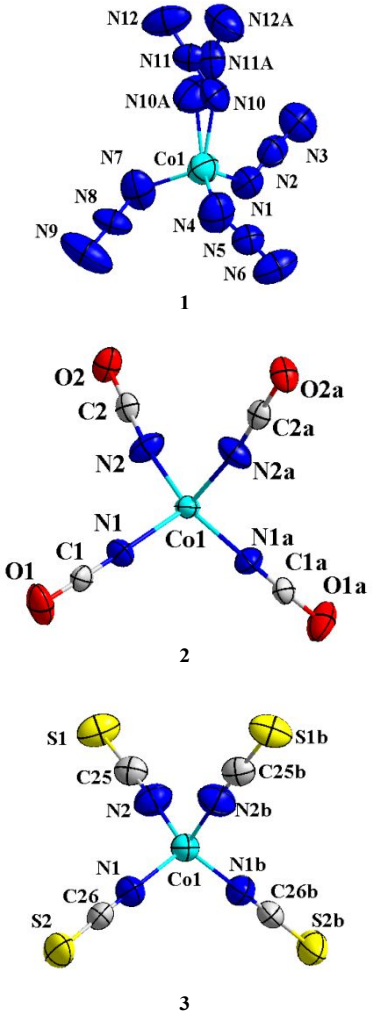

Fig. 1 Molecular structures of the anions of **1-3** (30% probability).

Table 2 Selected bond lengths (Å) and angles (°) for **1-3**

1		**2**		**3**	
Bond lengths		Bond lengths		Bond lengths	
Co(1)-N(1)	1.964 (4)	Co(1)-N(1)	1.956(2)	Co(1)-N(1)	1.943(2)
Co(1)-N(4)	1.995(4)	Co(1)-N(1)^a	1.956(2)	Co(1)-N(1)b	1.943(2)
Co(1)-N(7)	1.951(4)	Co(1)-N(2)	1.976(3)	Co(1)-N(2)	1.949(3)
Co(1)-N(10)	1.982(7)	Co(1)-N(2)^a	1.976(3)	Co(1)-N(2)b	1.949(3)
Co(1)-N(10A)	1.947(15)				
Bond angles		Bond angles		Bond angles	
N(1)-Co-N(4)	113.44(17)	N(1)-Co-N(1)^a	115.28(15)	N(1)-Co-N(1)^b	112.08(14)
N(1)-Co-N(7)	106.39(16)	N(1)^a-Co-N(2)^a	108.79(11)	N(1)-Co-N(2)^b	109.63(11)
N(1)-Co-N(10)	106.4(3)	N(1)-Co-N(2)^a	108.91(11)	N(1)^b-Co-N(2)^b	110.27(11)
N(1)-Co-N(10A)	104.8(7)	N(1)^a-Co-N(2)	108.91(11)	N(1)-Co-N(2)	110.27(11)
N(4)-Co-N(7)	104.69(16)	N(1)-Co-N(2)	108.79(11)	N(1)^b-Co-N(2)	109.63(11)
N(4)-Co-N(10)	106.9(3)	N(2)-Co-N(2)^a	105.74(17)	N(2)-Co-N(2)^b	104.72(15)
N(4)-Co-N(10A)	126.1(6)	N(1)-C(1)-O(1)	178.7(3)	N(2)-C(25)-S(1)	177.6(2)
N(7)-Co-N(10)	119.4(2)	N(2)-C(2)-O(2)	178.3(3)	N(1)-C(26)-S(2)	179.8(3)
N(7)-Co-N(10A)	99.0(7)	Co-N(1)-C(1)	176.2(3)	Co-N(1)-C(26)	172.4(3)
N(1)-N(2)-N(3)	177.4(4)	Co-N(2)-C(2)	172.0(3)	Co-N(2)-C(25)	174.7(2)
N(4)-N(5)-N(6)	172.7(4)				
N(7)-N(8)-N(9)	178.9(5)				
N(10)-N(11)-N(12)	177.7(9)				
N(10A)-N(11A)-N(12A)	167(3)				
Co-N(1)-N(2)	125.2(3)				
Co-N(4)-N(5)	134.8(3)				
Co-N(7)-N(8)	132.4(3)				
Co-N(10)-N(11)	131.9(8)				
Co-N(10A)-N(11A)	132(3)				

Symmetry codes: (*a*) –*x*+1, *y*, -*z*+3/2; (*b*) –*x*+1, *y*, -*z*+3/2

The N-Co-N bond angles vary from 99.0(7) to 119.4(2)° in **1**, 105.74(17) to 115.28(15)° in **2** and 104.72(15) to 112.08(14)° in **3**. These Co-N bond lengths and N-Co-N bond angles are similar to those of other reported tetra(pseudohalide)-cobalt(II) complexes.[10e-10h,17-19]

The most marked difference between **1** and **2-3** is the Co-N-X linkage. The Co-N-N linkage in **1** is significantly bent with the Co-N-N bond angles spanning the range of 125.2(3)-134.8(3)°, similar to those in early reported $(Ph_4P)_2[Co(N_3)_4]$,[19a] while the Co-N-C linkages in **2-3** are almost linear with the angles varying from 172.0(3) to176.2(3)° in **2** and from 172.4(3) to 174.7(2)° in **3**. The N_3^-, NCO^- and NCS^- ligands are also linear with the angles in the range 167(3)-178.9(5)° in **1**, 178.3(3)-178.7(3)° in **2**, and 177.6(2)-179.8(3)° in **3**. These bond parameters in **1-3** are close to those of complexes with different cations reported earlier.[10f,10h,17-19] The Co(II) ions are well-isolated with the shortest Co···Co distance of 10.22 Å, 7.51 Å and 8.12 Å for **1-3**, respectively.

To evaluate the deviation degree of the CoN_4 tetrahedra from the ideal T_d symmetry, continuous shape measurement (ChSM) analyses were performed for **1-3** and the reported analogues by using the SHAPE 2.1 program.[27] The calculated deviation parameter provides an estimation of the deviation from the ideal structure with 0 corresponding to the ideal polyhedron. The deviation parameters and their CSD refcodes of all reported examples of tetrakis(pseudohalido)-cobalt(II) complexes of the three anions, including **1-3**, are listed in Tables S2-S4. The calculated values relative to the ideal tetrahedron geometry are 0.297, 0.073 and 0.055 for **1-3**, respectively (Tables S2-S4). The deviation parameters calculated for $[Co(NCS)_4]^{2-}$ $[Co(NCO)_4]^{2-}$ and $[Co(N_3)_4]^{2-}$ are found to fall in the large range of 0.024-2.352, 0.016-0.184 and 0.107-0.960, respectively (Table S2-S4).[10e-10h,17-19] These various values found for the same anions suggest that the counter cation has a significant impact on the structural distortion of the anion, which might be ascribed to the effect of crystal packing. Such distortion caused by the counter cation might lead to the different magnetic properties.

Static magnetic properties

The temperature dependences of the molar magnetic susceptibility (χ_M) per Co(II) ion presented in the form of $\chi_M T$ vs T plots are shown in Fig. 2a and Figs. S4-S5. At 300 K, the $\chi_M T$ values of 2.51, 2.46, and 2.33 $cm^3 \cdot K \cdot mol^{-1}$ at 300 K for **1-3**, respectively, are consistent with an $S = 3/2$ spin center with g value of 2.31, 2.29, and 2.23. Each $\chi_M T$ product is significantly larger than the spin-only value of one isolated high spin Co(II) ion with $S = 3/2$, $g = 2.0$ (1.875 $cm^3 \cdot K \cdot mol^{-1}$). These values fall within the range of 2.1-3.4 $cm^3 \cdot K \cdot mol^{-1}$ reported for a single non-interacting d^7 Co(II) ion with a considerable contribution

from orbital angular momentum.[5-16,28] On cooling from 300 K, the $\chi_M T$ product remains nearly constant to 90 (**1**), 30 (**2**), and 25 K (**3**) and then significantly decreases to a minimum value of 1.62, 1.77, and 1.74 $cm^3 \cdot K \cdot mol^{-1}$ at 2.0 K, respectively. Such a turndown in low temperature range is mainly due to the intrinsic magnetic anisotropy of the Co(II) ion in **1**-**3**.

The magnetizations for **1**-**3** at 7 T and 1.8 K are 2.36, 3.11, and 3.15 $N_A\mu_B$, respectively, none of which has reached saturation. The unsaturation of magnetization at 7 T and the non-superposition of M vs B/T curves at various applied dc fields and 1.8-5.0 K (Fig. 2b and Figs. S4-S5) further indicate the presence of considerable magnetic anisotropies in **1**-**3**.

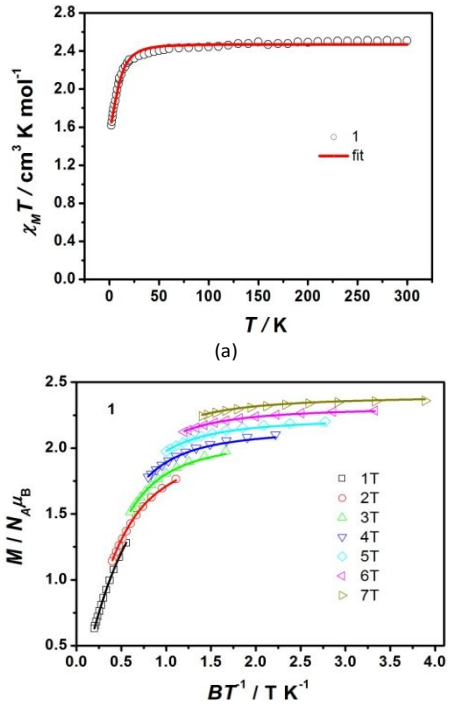

Fig. 2 (a) Variable-temperature dc susceptibility under an applied dc field of 0.1 T for **1**. (b) Variable-temperature, variable-field dc magnetization data of **1**. Fields of 1-7 T were used at temperatures from 1.8 K to 5.0 K. Solid lines are the best fits with *PHI* program.[29]

For the four-coordinate Co(II) complexes, the ZFS parameters D and E can be used to describe their magnetic anisotropies. To estimate D and E values, the $\chi_M T$ vs T and M vs B/T curves were simultaneously analyzed by using *PHI* program,[29] with the spin Hamiltonian given in Eqn (1):

$$\hat{H} = D(\hat{S}_z^2 - S(S+1)/3) + E(\hat{S}_x^2 - \hat{S}_y^2) + \mu_B g \hat{S} B \qquad (1)$$

in which μ_B denotes the Bohr magneton, D, E, S and B represent the axial and rhombic ZFS parameters, spin, and magnetic field vector, respectively. Intermolecular interactions were considered as molecular field correction zJ. For **1**, reasonable results were obtained only when the sign of D was assigned to be negative (Fig. 2). However, the fitting of magnetic data of **2**-**3** could not define the sign for the D values as both sets of parameters with negative and positive D values can give reasonable fits. The sign of D values was determined to be negative for **2** and positive for **3** by HFEPR and theoretical calculations (vide infra), giving the D values in Table 3. The magnitude of D value of **1** is larger than those of **2** and **3**, probably due to the high degree of structural distortion in **1**, as shown in the larger derivation parameter of **1** in the ChSM analyses.

Table 3 The fitting parameters from the direct-current magnetic data for **1**-**3**

	D, cm^{-1}	E, cm^{-1}	$g_{x,y}$	g_z	zJ, cm^{-1}
1	-12.11(5)	0.49(7)	2.272(3)	2.338(2)	0.00185(7)
2	-4.97(1)	0.05(4)	2.264(2)	2.331(2)	-0.0158(9)
3	3.86(0)	0.14(2)	2.263(0)	2.258(1)	-0.00876(8)

HFEPR Studies

HFEPR spectroscopy[30] was used to further study the nature of magnetic anisotropies of **1**-**3**. The HFEPR spectra were recorded for the powder samples of **1**-**3** with different frequencies and magnetic fields (Fig. S6 and Figs. 3-4). There is no obvious EPR signal for **1** (Fig. S6). However, several resonance signals are observed for **2** and **3** at 2 K or 10 K at different frequencies.

In a high-spin Co(II) complex, there are two types of possible EPR transitions: intra-Kramers, *i.e.*, the transitions within Ms = ±1/2 states, and inter-Kramers transitions, *i.e.* those occurring between the two Kramers doublets. When the Ms = ±3/2 Kramers doublet lies at lower energy than the Ms = ±1/2 doublet, corresponding to easy-axis magnetic anisotropy, the intra-Kramers transition within the ±3/2 doublet, corresponding to ΔMs = ±3, is nominally forbidden. This transition could be partly allowed when a sizable rhombic ZFS E term mixes the Ms = ±3/2 doublet with the Ms = ±1/2 doublet. In contrast, the inter-Kramers transition between the Ms = ±3/2 Kramers doublet and the Ms = ±1/2 doublet is possible when the energy separation is smaller than the microwave energy used in HFEPR. The absence of HFEPR signal in **1** suggests that the magnetic anisotropy is easy-axial and zero-field splitting $2(D^2 + 3E^2)^{1/2}$ exceeds the frequency range in our measurements (~13.3 cm^{-1}).

In the HFEPR spectrum of **2** at 324 GHz (Fig. 3), a resonance near zero field gives a roughly estimated value for $2(D^2 + 3E^2)^{1/2}$ as 10.8 cm^{-1}. Then D = 5.4 cm^{-1} and E = 0 were used as the initial values for the simulations. The two-dimensional (2D) map of resonance fields at various frequencies was established and showed in Fig. 3b, where the transitions are plotted as squares. All experimental points can be simulated by the spin Hamiltonian (Eqn 1) with the program Spin.[31] The derived spin Hamiltonian parameters are $|D|$ = 5.23 cm^{-1}, E = 0.056 cm^{-1}, g_{xy} = 2.2, and g_z = 2.18. In order to reveal the sign of D value, the EPR spectrum recorded at 324.0 GHz and 2 K was also simulated using the above Hamiltonian parameters (Fig. 3a). The comparison of the experimental spectrum to the simulated spectra (using the positive and negative D values) shows the D value for **1** is negative.

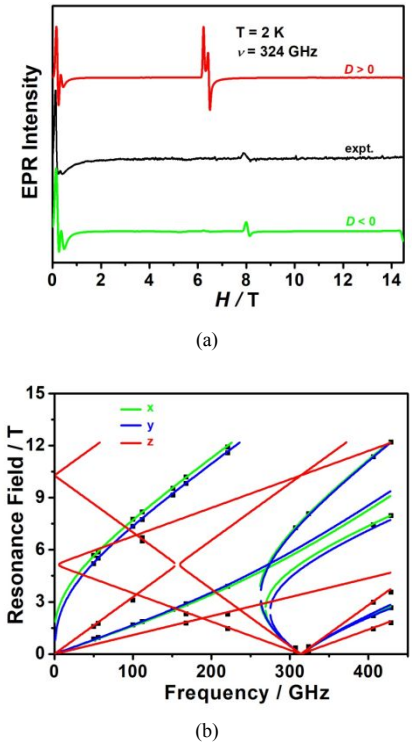

(a)

(b)

Fig. 3 (a) HFEPR spectrum of **2** at 2 K (black) and its simulations (red trace: positive *D*; green trace: negative *D*) at 324 GHz; (b) Resonance field vs microwave frequency for EPR transitions for **2**. Simulations were conducted by program Spin.[31] Solid lines show the (*x, y, z*) transitions as labelled.

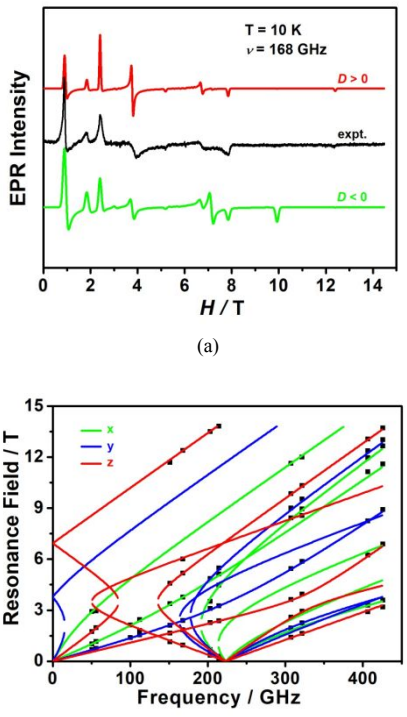

(a)

(b)

Fig. 4 (a) HFEPR spectrum of **3** at 10 K (black) and its simulations (red trace: positive *D*; green trace: negative *D*) at 168 GHz; (b) Resonance field vs microwave frequency for EPR transitions for **3**. Simulations were conducted by the program Spin.[31] Solid lines show the (*x, y, z*) transitions as labelled.

A typical EPR spectrum of **3** at 10 K with 168 GHz is shown in Fig. 4a. A 2D map of resonance fields at various microwave frequencies was plotted in Fig. 4b and was simulated by spin Hamiltonian (Eqn 1) with the program Spin.[30] The derived spin Hamiltonian parameters are $|D| = 3.63$ cm^{-1}, $E = 0.49$ cm^{-1}, $g_{xy} = 2.27$, and $g_z = 2.22$. The positive sign of *D* value was confirmed by the comparison between the experimental spectrum at 168 GHz and the simulated spectra using both the negative and positive *D* values (Fig. 4b).

The Hamiltonian parameters obtained from HFEPR spectra can be used to simulate the magnetic curves. The calculated $\chi_M T$ versus *T* plots and *M-B/T* curves are in good agreement with the experimental ones (Fig. S7-S8)

As shown in Table 1, the complexes with the $[Co(NCS)_4]^{2-}$ anion have positive *D* values. *D* value of **3** (+3.63 cm^{-1}) is in the range of those reported for $[Co(NCS)_4]^{2-}$ analogues (+2.57 – +11.6 cm^{-1}) (Table 1).[10e-10h] The *D* value of -5.23 cm^{-1} for **2** is different from the reported value of +4.3 cm^{-1} for $[Co(tppz)_2][Co(NCO)_4].2H_2O$.[10h] The various *D* values for the same anion, but different cations, may be the result of the structural distortions caused by the counter cations.

To conclude, HFEPR spectra showed the easy-axis anisotropy for **1** and **2** but easy-plane anisotropy for **3**. The larger magnitude of *D* in **1** prevented its exact determination, but a negative sign was deduced.

Dynamic magnetic properties

The ac susceptibility measurements were performed for **1-3** to study the dynamic magnetic behaviors at the low temperatures. No out-of-phase ac susceptibility (χ_M") signal was observed under zero applied dc field at 1.8 K (Fig. S9), which could be due to the occurrence of quantum tunnelling of the magnetization (QTM). When an external dc field was applied, these complexes showed frequency-dependent out-of-phase χ_M" signals, indicating that the application of a dc field would efficiently suppress the QTM and induce non-zero χ_M" signals. A peak of χ_M" appeared at 0.02 T for **1** and shifted to low frequencies and then remained nearly constant at the same frequency. The peak reached the maximum at 0.08 T. Similarly, a maximum of χ_M" of **2** was found when a field of 0.02 T was applied. The maximum shifted to low frequencies and the moving speed became slow after 0.10 T, but the maximum value of χ_M" decreased sharply. In contrast, no maximum of χ_M" was observed for **3**, but the intensities of χ_M" signals gradually enhanced with the increasing of the applied magnetic field. Magnetic field of 0.08 T for **1**, 0.10 T for **2** and **3** were then chosen for further temperature- and frequency-dependent ac measurements at 1.8-5.0 K (Figs. 5-7). Temperature-dependent χ_M" signals were observed below 2.6 K (**1**), 4.0 K (**2**) and 4.5 K (**3**) as shown in χ_M" vs *T* plots (Figs. S10-S12). These data confirm that **1-3** exhibit field-induced slow magnetic relaxation.

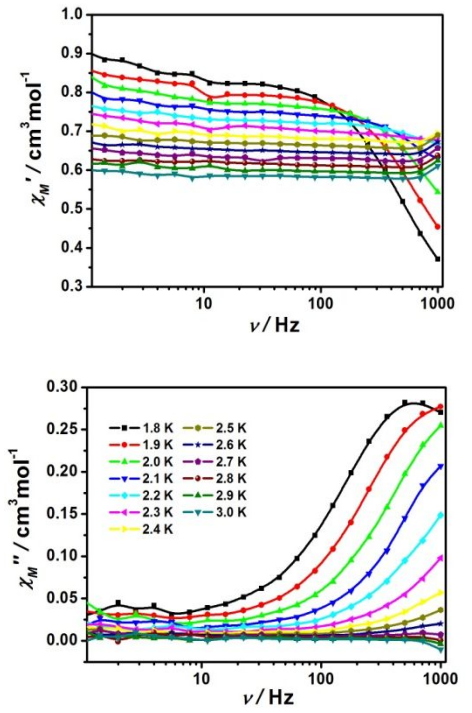

Fig. 5 Frequency dependence of in-phase (χ_M') and out-of-phase (χ_M'') ac magnetic susceptibilities from 1.8 to 3.0 K under 0.08 T dc field for **1**. The solid lines are for eye guide.

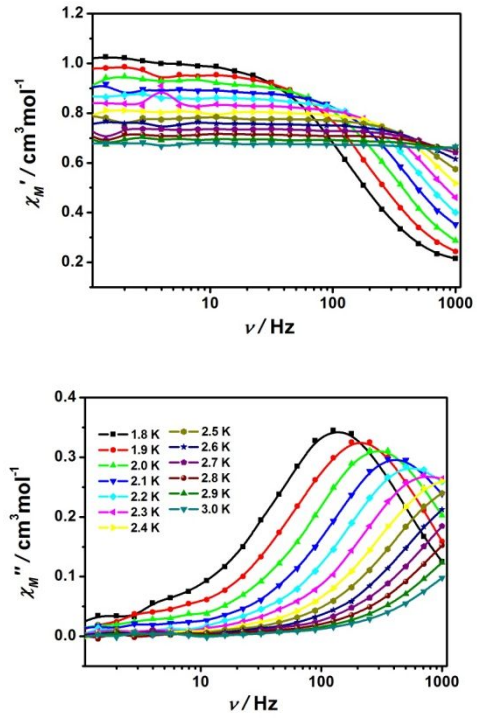

Fig. 6 Frequency dependence of in-phase (χ_M') and out-of-phase (χ_M'') ac magnetic susceptibilities from 1.8 to 3.0 K under 0.10 T dc field for **2**. The solid lines are for eye guide.

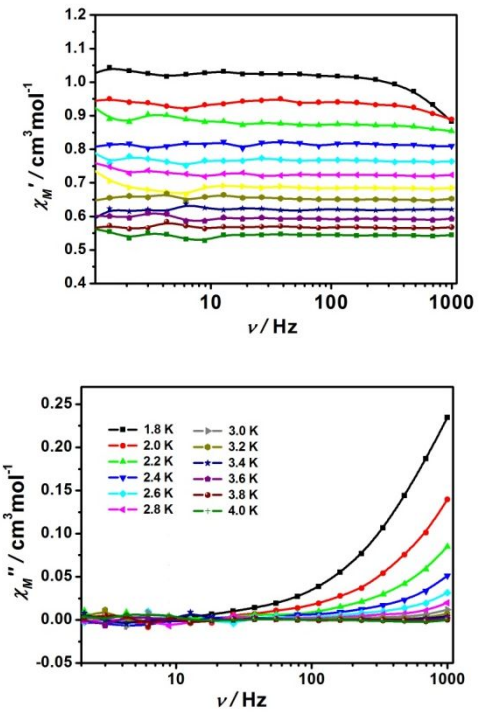

Fig. 7 Frequency dependence of in-phase (χ_M') and out-of-phase (χ_M'') ac magnetic susceptibilities from 1.8 to 4.0 K under 0.1 T dc field for **3**. The solid lines are for eye guide.

To determine the relaxation times at different temperatures, the Cole-Cole plots for **2** were constructed in the range of 1.8-2.6 K (Fig. S13) which were fitted with the generalized Debye model by Eqn (2):[32]

$$\chi_{ac}(\omega) = \chi_S + \frac{\chi_T - \chi_S}{1 + (i\omega\tau)^{(1-\alpha)}} \qquad (2)$$

The fitting parameters of χ_T (isothermal susceptibility), χ_S (adiabatic susceptibility), τ (relaxation time) and α (deviation from a pure Debye model) are summarized in Table S6. The resulting parameters α are in the range of 0.09-0.13 for **2**, indicating that the distribution of relaxation times is very small and only one relaxation process is present.

If a SIM supposedly has only one characteristic time, corresponding to an Orbach relaxation process with one activation energy (U_{eff}), the relaxation time (τ) may be written in terms of the Arrhenius law $\tau = \tau_0 \exp(U_{eff}/k_BT)$. The τ values of **2** extracted from the Debye model were fit to give $U_{eff} = 10.5$ cm^{-1} and $\tau_0 = 3.63 \times 10^{-7}$ s (Fig. S14). The effective energy barrier of **2** is consistent with the $2(D^2+3E^2)^{1/2}$ value (10.8 cm^{-1}) expected for an Orbach process.

For **1** and **3**, only one or no χ_M'' peak was observed (Figs. 5 and 7), preventing us to further analyze the relaxation processes. It is obvious that the magnetic relaxation in **1** and **3** is much faster than **2**.

Theoretical studies of magnetic anisotropies in 1–3

In order to gain further insight into magnetic anisotropies in **1**−**3** with different pseudo-halides, *ab initio* calculations were performed for the experimentally determined structures of **1**−**3** (Fig. S15) using complete-active-space self-consistent field (CASSCF) with MOLCAS 8.2[33] and N-electron valence second-order perturbation theory (NEVPT2) approach with ORCA 4.2.[34–38] Calculation details are given in ESI.

The calculated energies of the spin-free states and spin-orbit states are listed in Tables S7-S8. The first excited spin-free state is in the range of 3370.6−4468.1 cm^{-1} above the ground one in **1**−**3**, suggesting that the lowest quartet term is well isolated from the excited ones. The energy differences between the lowest two spin-free states (Table S7) of **1**−**3** are much larger than those between the lowest two spin-orbit states (Table S8). Furthermore, the lowest two spin-orbit states in **1**−**3** are almost composed of the ground spin-free one. These are consistent with the orbital nondegeneracy of the ground term in **1**−**3**, which allowed us to use spin Hamiltonian (Eqn 1) with the ZFS parameters *D* and *E* to model their magnetic anisotropies. The calculated *D*, *E* (cm^{-1}) and *g* (g_x, g_y, g_z) tensors for **1**−**3** using CASSCF[33] and NEVPT2[38] are shown in Table 4. The calculated *D* values using both approaches are negative for **1**−**2** and positive for **3**. These calculated *D*(*E*) values are close to those determined by HFEPR.

Table 4. Calculated ZFS parameters *D*, *E* (cm^{-1}) and ***g*** (g_x, g_y, g_z) tensors of the lowest spin-orbit states of **1**−**3** using CASSCF and NEVPT2 with MOLCAS 8.2 and ORCA 4.2, respectively

	CASPT2				
	D_{cal}	E_{cal}	g_x	g_y	g_z
1	−10.8	–0.61	2.229	2.348	2.369
2	−3.4	−0.05	2.268	2.271	2.306
3	+2.0	+0.03	2.264	2.261	2.242
	NEVPT2				
	D_{cal}	E_{cal}	g_x	g_y	g_z
1	−6.5	–2.10	2.001	2.087	2.153
2	−3.2	+0.15	2.243	2.244	2.276
3	+2.0	+0.08	2.238	2.232	2.216

To deeply analyze the magnetic anisotropies, we obtained the contributions of the excited states to *D* values of **1**−**3** in Table S9 using NEVPT2 with ORCA 4.2.[38] The dominant contributions to the negative *D* values of **1** and **2** were found to arise from the two close quartet states, particularly the first and the second quartet states for **1** and the first and the third quartet states for **2**. The dominant contributions to the positive *D* value of **3** were found to be from the three close quartet states.

The sign and value of *D* can be rationalized using a spin-orbit coupling operator.[39-40] When the spin-conserved excitation occurs between orbitals with the same $|m_l|$ values, the *M*s = ±3/2 components become more stable, and thus a negative contribution to the *D* value is expected. On the other hand, an excitation between orbitals involving a $\Delta|m_l| = 1$ change, which produces the stabilized *Ms* = ±1/2 components, leads to a positive contribution to the *D* value.[39-40] The calculated relative energy order (cm^{-1}) of ligand field one-electron states (in the basis of *d*-atomic orbitals (*d*-AOs)) for **1**−**3** has been extracted using NEVPT2 with ORCA 4.2 according to the *ab initio* ligand field theory (AILFT) analysis[41–42] (Table S10). The orbital energies computed for the ground state are shown in Fig. S16, where the ground state for **1** has a dominant (92.2%) $(d_{x^2-y^2})^1(d_{z^2})^1(d_{yz})^2(d_{xz})^1(d_{xy})^2$ configuration. The ground states for **2** and **3** are both multideterminant with prevailing (72.1% and 59.1%, respectively) contribution of $(d_{x^2-y^2})^1(d_{xz})^1(d_{xy})^1(d_{yz})^2(d_{z^2})^2$ and $(d_{xz})^1(d_{x^2-y^2})^1(d_{z^2})^1(d_{xy})^2(d_{yz})^2$, and are mixed with each other with the weightage of 27.6% and 25.6%, respectively. For **3**, the major contributions to *D* are from the ground to the first and third excited states transitions ($d_{xy}\rightarrow d_{z^2}$ and $d_{yz}\rightarrow d_{x^2-y^2}$, respectively; see Figs. S16 and S17). The positive sign of the *D* parameter is attributed to these transitions, which occur between the orbitals with the different magnetic quantum number (m_l) values.[39–40]

The calculated $\chi_M T$ versus *T* plots of **1**−**3** are shown in Fig. S18. The calculated g_x, g_y, and g_z orientations of the ground spin-orbit states on Co(II) ions of **1**−**3** are shown in Fig. S19.

Conclusions

In this paper, we have present the syntheses, structures and magnetic properties of three tetrakis(pseudohalido)-cobalt(II) complexes $(Ph_4P)_2[Co(E)_4]$ (E = N_3^-, **1**; NCO^-, **2**; NCS^-, **3**). The structural determinations show that the central anionic CoN_4 moiety adopts a distorted tetrahedron in **1-3**. The detailed dc magnetic measurements and HFEPR studies indicated the sensitivity of the magnetic anisotropy varying with the nature of the ligands. Easy-axis magnetic anisotropy was found for **1** and **2** but easy-plane anisotropy for **3**, which is supported by the *ab initio* calculations. According to the ac magnetic susceptibilities, the three complexes exhibit slow magnetic relaxation under an applied field and thus are field-induced SIMs. The current work adds three new numbers to the mononuclear tetrahedral Co(II) SIMs family.

Conflicts of interest

There are no conflicts to declare.

Author contributions

Shu-Yang Chen: synthesis, characterization, structural determination and manuscript writing; Wei Lv, Hui-Hui Cui: magnetic measurement and modelling; Zhenxing Wang, Zhong-Wen Ouyang, Lei Chen: HFEPR measurements and interpretations; Yi-Quan Zhang: theoretical calculations and interpretations; Xue-Tai Chen, Hong Yan, Zi-Ling Xue: project design and writing.

Acknowledgements

We are grateful for the financial support from the Natural Science Grant of China (No. 21471078 to XTC, No, 11774178 to YQZ), and

the US National Science Foundation (CHE-1900296 and CHE-2055499 to ZLX). A portion of this work was performed at the National High Magnetic Field Laboratory, which is supported by the National Science Foundation through NSF/DMR-1644779 and the State of Florida.

Notes and references

1 (*a*) D. Gatteschi, R. Sessoli and J. Villain, *Molecular Nanomagnets*, Oxford University Press, Oxford, UK, 2006; (*b*) P. C. E. Stamp and A. Gaita-Arino, *J. Mater. Chem*., 2009, **19**, 1718; (*c*) W. Wernsdorfer and R. Sessoli, *Science*, 1999, **284**, 133; (*d*) M. N. Leuenberger and D. Loss, *Nature*, 2001, **410**, 789.

2 R. Sessoli, H. L. Tsai, A. R. Schake, S. Wang, J. B. Vincent, K. Folting, D. Gatteschi, R. Sessoli, G. Christou and D. N. Hendrickson, *J. Am. Chem. Soc.*, 1993, **115**, 1804.

3 F. Neese, D. A. Pantazis, *Faraday Discuss.* 2011, **148**, 229.

4 (*a*) D. N. Woodruff, R. E. P. Winpenny and R. A. Layfield, *Chem. Rev.*, 2013, **113**, 5110; (*b*) F.-S. Guo, B. M. Day, Y.-C. Chen, M.-L. Tong, A. Mansikkamäki, R A. Layfield, *Science*, 2018, 362, 1400.,

5 (*a*) M. Feng and M.-L. Tong, *Chem. Eur. J.* 2018, **24**, 7574; (*b*) G. A. Craig and M. Murrie, *Chem. Soc. Rev*., 2015, **44**, 2135; (*c*) A. K. Bar, C. Pichon and J.-P. Sutter, *Coord. Chem. Rev.*, 2016, **308**, 346; (*d*) J. M. Frost, K. L. M. Harriman and M. Murugesu, *Chem. Sci.*, 2016, **7**, 2470; (e) A. Sarkar, S. Dey, and G. Rajaraman, *Chem. Eur. J.* 2020, **26**, 14036.

6 P. C. Bunting**,** M. Atanasov, E. Damgaard-Møller, M. Perfetti, I. Crassee, M. Orlita, J. Overgaard, J. V. Slageren, F. Neese and J. R. Long, *Science*, 2018, **362**, 1.

7 F. Deng, T. Han, B. Yin and Y.-Z. Zheng, *Inorg. Chem. Front.*, 2017, **4**, 1141.

8 (*a*) S. Ziegenbalg, D. Hornig, H. Görls, W. Plass, *Inorg. Chem.* 2016, **55**, 4047; (*b*) S. Vaidya, A. Upadhyay, S. K. Singh, T. Gupta, S. Tewary, S. K. Langley, J. P. S. Walsh, K. S. Murray, G. Rajaraman and M. Shanmugam, *Chem. Commun.*, 2015, **51**, 3739; (*c*) L. Smolko, J. Černák, M. Dušek, J. Miklovič, J. Titiš and R. Boča, *Dalton Trans*., 2015, **44**, 17565; (*d)* L. Smolko, J. Černák, M. Dušek, J. Titiš and R. Boča, *New J. Chem.***,** 2016, **40**, 6593; *(e)* L. Smolko**,** J. Černák, J. Kuchár, C. Rajnák, J. Titiš and R. Boča, *Eur. J. Inorg. Chem.*, 2017, ***24***, 3086; (*f*) A. Switlicka, B. Machura, R. Kruszynski, J. Cano, L. M. Toma, F. Lloret and M. Julve, *Dalton Trans.*, 2018, **47**, 5831; (g) S. Vaidya, P. Shukla, S. Tripathi, E. Rivière, T. Mallah, G. Rajaraman and M. Shanmugam, *Inorg. Chem.*, 2018, **57**, 3371.

9 (*a*) J. M. Zadrozny and J. R. Long, *J. Am. Chem. Soc*., 2011, **133**, 20732; (*b*) J. M. Zadrozny, J. Telser and J. R. Long, *Polyhedron,* 2013, **64**, 209; (*c*) E. A. Suturina, J. Nehrkorn, J. M. Zadrozny, J. Liu, M. Atanasov, T. Weyhermüller, D. Maganas, S. Hill, A. Schnegg, E. Bill, J. R. Long and F. Neese, *Inorg. Chem*., 2017, **56**, 3102; (*d*) M. S. Fataftah, J. M. Zadrozny, D. M. Rogers and D. E. Freedman, *Inorg. Chem.*, 2014, **53**, 10716; (*e*) M. S. Fataftah, S. C. Coste, B. Vlaisavljevich, J. M. Zadrozny and D. E. Freedman, *Chem. Sci*., 2016, **7**, 6160; (*f*) S. Vaidya, S. Tewary, S. K. Singh, S. K. Langley, K. S. Murray, Y. Lan, W. Wernsdorfer, G. Rajaraman and M. Shanmugam, *Inorg. Chem*., 2016, **55**, 9564; (*g*) S. Sottini, G. Poneti, S. Ciattini, N. Levesanos, E. Ferentinos, J. Krzystek, L. Sorace and P. Kyritsis, *Inorg. Chem*., 2016, **55**, 9537; (*h*) D. Tu, D. Shao, H. Yan and C. Lu, *Chem. Commun*., 2016, **52**, 14326; (*i*) D. R. Alcoba, O. B. Oña, G. E. Massaccesi, A. Torre, L. Lain, J. I. Melo, J. E. Peralta and J. M. Oliva-Enrich, *Inorg. Chem*., 2018, **57**, 7763; (*j*) K. Chattopadhyay, M. J. H. Ojea, A. Sarkar, M. Murrie, G. Rajaraman and D. Ray, *Inorg. Chem.*, 2018, **57**, 13176; (*k*) X.-N. Yao, M.-W. Yang, J. Xiong, J.-J. Liu, C. Gao, Y.-S. Meng, S.-D. Jiang, B.-W. Wang and S. Gao, *Inorg. Chem. Front.*, 2017, **4**, 701.

10 (*a*) Y. Rechkemmer, F. D. Breitgoff, M. van der Meer, M. Atanasov, M. Hakl, M. Orlita, P. Neugebauer, F. Neese, B. Sarkar and J. van Slageren, *Nature Commun*., 2016, **7**, 1; (*b*) E. Carl, S. Demeshko, F. Meyer and D. Stalke, *Chem. Eur. J*., 2015, **21**, 10109; (*c*) J. Vallejo, E. Pardo, M. Viciano-Chumillas, I. Castro, P. Amorós, M. Déniz, C. Ruiz-Pérez, C. Yuste-Vivas, J. Krzystek, M. Julve, F. Lloreta and J. Cano, *Chem. Sci*., 2017, **8**, 3694; (*d*) R. Bruno, J. Vallejo, N. Marino, G. D. Munno, J. Krzystek, J. Cano, E. Pardo and D. Armentano, *Inorg. Chem*., 2017, **56**, 1857; (*e*) Y.-Y. Zhu, F. Liu, J.-J. Liu, Y.-S. Meng, S.-D. Jiang, A.-L. Barra, W. Wernsdorfer and S. Gao, *Inorg. Chem*., 2017, **56**, 697; (*f*) L. H. G. Kalinke, J. C. O. Cardoso, R. Rabelo, A. K. Valdo, F. T. Martins, J. Cano, M. Julve, F. Lloret and D. Cangussu, *Eur. J. Inorg. Chem.*, 2018, 816; (*g*) D. Shao, L.-D. Deng, L. Shi, D.-Q. Wu, X.-Q. Wei, S.-R. Yang, and X.-Y. Wang, *Eur. J. Inorg. Chem.*, 2017, 3862; (*h*) J. Palion-Gazda, B. Machura, R. Kruszynski, T. Grancha, N. Moliner, F. Lloret, and M. Julve, *Inorg. Chem.*, 2017, **56**, 6281.

11 (*a*) A. Piecha-Bisiorek, A. Bieńko, R. Jakubas, R. Boča, M. Weselski, V. Kinzhybalo, A. Pietraszko, M. Wojciechowska, W. Medycki and D. Kruk, *J. Phys. Chem. A*, 2016, **120**, 2014; (*b*) O. Y. Vassilyeva, E. A. Buvaylo, V. N. Kokozay, B. W. Skelton, C. Rajnák, J. Titiš and R. Boča, *Dalton Trans*., 2019, **48**, 11278.

12 T. Jurca, A. Farghal, P. -H. Lin, I. Korobkov, M. Murugesu and D. S. Richeson, *J. Am. Chem. Soc.*, 2011, **133**, 15814; (*b*) D. Schweinfurth, M. G. Sommer, M. Atanasov, S. Demeshko, S. Hohloch, F. Meyer, F. Neese and B. Sarkar, *J. Am. Chem. Soc.*, 2015, **137**, 1993.

13 (a) J. Vallejo, I. Castro, R. Ruiz-García, J. Cano, M. Julve, F. Lloret, G. De Munno, W. Wernsdorfer and E. Pardo, *J. Am. Chem. Soc*., 2012, **134**, 15704; (b) D. H. Moseley, S. E. Stavretis, K. Thirunavukkuarasu, M. Ozerov, Y. Cheng, L. L. Daemen, J. Ludwig, Z. Lu, D. Smirnov, C. M. Brown, A. Pandey, A. J. Ramirez-Cuesta, A. C. Lamb, M. Atanasov, E. Bill, F. Neese and Z.-L. Xue, *Nat. Commun.* 2018, **9**, 2572.

14 X.-C. Huang, C. Zhou, D. Shao and X.–Y. Wang, *Inorg. Chem*., 2014, **53**, 12671.

15 (*a*) L. Chen, J. Wang, J.-M. Wei, W. Wernsdorfer, X.-T. Chen, Y.-Q. Zhang, Y. Song and Z.-L. Xue, *J. Am. Chem. Soc*., 2014, **136**, 12213; (*b*) S. E. Stavretis, D. H. Moseley, F. Fei, H.-H. Cui, Y. Cheng, A. A. Podlesnyak, X. Wang, L. L. Daemen, C. M. Hoffmann, M. Ozerov, Z. Lu, K. Thirunavukkuarasu, D. Smirnov, T. Chang, Y.-S. Chen, A. J. Ramirez-Cuesta, X.-T. Chen, Z.-L. Xue, *Chem. Eur. J.* 2019, **25**, 15846.

16 J. Krzystek, D. C. Swenson, S. A. Zvyagin, D. Smirnov, A. Ozarowski and J. Telser, *J. Am. Chem. Soc.*, 2010, **132**, 5241.

17 The deviation parameres from ChSM analysis for the Known $[Co(NCS)_4]^{2-}$ anions are listed in Table S4 (ESI). Also see Refences S33-S119 (ESI).
18 The deviation parameres from ChSM analysis for the Known $[Co(NCO)_4]^{2-}$ anions are listed in Table S3 (ESI). Also see Refences S26-S32 (ESI).
19 The deviation parameres from ChSM analysis for the known $[Co(N_3)_4]^{2-}$ anions are listed in Table S2 (ESI). (*a*) R. Sen, A. Mondal, *J. Mol. Struct.*, 2019, **1198**, 126882; (*b*) S. S. Massoud, M. Dubin, A. E. Guilbeau, M. Spell, R. Vicente, P. Wilfling, R. C. Fischer and F. A. Mautner, *Polyhedron*, 2014, **78**, 135.
20 R. Boča, J. Titiš, C. Rajnák and J. Krzystek, *Dalton Trans*., 2021, **50**, 3468.
21 A. K. Hassan, L. A. Pardi, JKrzystek, A. Sienkiewicz, P. Goy, M. Rohrer, L.-C. Brunel, *J. Magn. Reson*., 2000, **142**, 300.
22 E. Styczeń, Z. Warnke and D. Wyrzykowski, *Thermochim. Acta*, 2007, **454**, 84.
23 *SAINT Software Users Guide*, Version 7.0, Bruker Analytical X-ray Syst*ems, Madison*, 1999.
24 G. M. Sheldrick, *SADABS*, Version 2.03, Bruker Analytical X-ray Systems, Madison, 2000.
25 G. M. Sheldrick, *Acta Crystallogr*., 2015, **C71**, 3.
26 G. A. Bain and J. F. Berry, *J. Chem. Educ.*, 2008, **85**, 532.
27 (*a*) M. Llunell, D. Casanova, J. Cirera, P. Alemany and S. Alvarez, *Shape Program*, Version 2.1, 2013; (*b*) S. Alvarez, P. Alemany, D. Casanova, J. Cirera, M. Llunell and D. Avnir, *Coord. Chem. Rev.,* 2005, **249**, 1693.
28 F. E. Mabbs and D. J. Machin, *Magnetism and Transition Matal Complexes*, Dover Publications: Mineola, NY, 2008.
29 N. F. Chilton, R. P. Anderson, L. D. Turner, A. Soncini and K. S. Murray, *J. Comput. Chem*., 2013, **34**, 1164.
30 (a) J. Krzystek, O. Ozarowski and J. Telser, *Coord. Chem. Rev.*, 2006, **250**, 2308; (b) J. Krzystek, S. A. Zvyagin, O. Ozarowski, S. Trofimenko and J. Telser, *J. Magn. Reson.*, 2006, **178**, 174.
31 Simulations were performed using SPIN developed by Andrew Ozarowski at the National High Magnetic Field Laboratory, USA.
32 (*a*) Y.-N. Guo, G.-F. Xu, Y. Guo and J. Tang, *Dalton Trans.*, 2011, **40**, 9953; (*b*) K. S. Cole and R. H. Cole, *J. Chem. Phys*., 1941, **9**, 341.
33 F. Aquilante, J. Autschbach, R. K. Carlson, L. F. Chibotaru, M. G. Delcey, L. De Vico, I. Fdez. Galván, N. Ferré, L. M. Frutos, L. Gagliardi, M. Garavelli, A. Giussani, C. E. Hoyer, G. Li Manni, H. Lischka, D. Ma, P. Å. Malmqvist, T. Müller, A. Nenov, M. Olivucci, T. B. Pedersen, D. Peng, F. Plasser, B. Pritchard, M. Reiher, I. Rivalta, I. Schapiro, J. Segarra-Martí, M. Stenrup, D. G. Truhlar, L. Ungur, A. Valentini, S. Vancoillie, V. Veryazov, V. P. Vysotskiy, O. Weingart, F. Zapata and R. Lindh, *J. Comput. Chem*., 2016, **37**, 506.
34 C. Angeli, R. Cimiraglia, S. Evangelisti, T. Leininger and J. P. Malrieu, *J. Chem. Phys.*, 2001, **114**, 10252.
35 C. Angeli, R. Cimiraglia and J.-P. Malrieu, *Chem. Phys. Lett.*, 2001, **350**, 297.
36 C. Angeli and R. Cimiraglia, *Theor. Chem. Acc.*, 2002, **107**, 313.
37 C. Angeli, R. Cimiraglia and J.-P. Malrieu, *J. Chem. Phys.*, 2002, **17**, 9138.
38 F. Neese, ORCA–*an ab initio, density functional and semiempirical program package*, Version 4.2; Max-Planck institute for bioinorganic chemistry: Mülheim an der Ruhr, Germany, 2019.
39 S. Gómez-Coca, E. Cremades, N. Aliaga-Alcalde and E. Ruiz, *J. Am. Chem. Soc*., 2013, **135**, 7010.
40 S. Gómez-Coca, D. Aravena, R. Morales and E. Ruiz, Coord. *Chem. Rev*., 2015, **289**, 379.
41 M. Atanasov, D. Ganyushin, K. Sivalingam and F. Neese, in *Molecular Electronic Structures of Transition Metal Complexes II*, eds. D. M. P. Mingos, P. Day and J. P. Dahl, Springer Berlin Heidelberg, Berlin, Heidelberg, 2012, pp. 149.
42 S. K. Singh, J. Eng, M. Atanasov and F. Neese, *Coord. Chem. Rev.*, 2017, **344**, 2.